

A hardware development for optical tomography system using switch mode fan beam projection

R. Abdul Rahim*, K.S. Chan, J.F. Pang, L.C. Leong

Process Tomography Research Group (PROTOM), Department of Control and Instrumentation Engineering, Faculty of Electrical Engineering, Universiti Teknologi Malaysia, 81310 UTM Skudai, Johor, Malaysia

Received 18 May 2004; received in revised form 29 October 2004; accepted 28 November 2004

Available online 19 February 2005

Abstract

This research used 16 pairs of optical sensors. The working principle is based on the switch and measure principle in electrical capacitance tomography (ECT), and fan beam shape projection from light emitters. The fast setting time of optical sensors and wide coverage of optical beam become the is implemented in a tomography system. In general, the system can be divided to three subsystems; they are projection, sensor signal conditioning and data acquisition. In the projection subsystem, a 4.8 kHz clock has been used to drive the LEDs, as a result, 300 complete projections obtained in a second. In the signal conditioning subsystem, a current to voltage converter has been used with each photodiode output, the signals are filtered and amplified before interfacing with the data acquisition system. In the data acquisition system, a computer based data acquisition system has been utilized. The modulated clocks from the projection sub-system are used to control the operation of data acquisition. This paper will discuss the detail of hardware development and shows the result obtained from the designed hardware system.

© 2004 Elsevier B.V. All rights reserved.

Keyword: Optical tomography

1. Introduction

Numerous types of optical tomography systems have been designed for process tomography. The designed systems involve the implementation of infrared sensor [1] as well as optical fiber sensor [2–4]. The systems designed by Dugdale, Abdul Rahim and Rzasz applied the parallel projection technique by arranging two projections perpendicularly while Ibrahim carried out the an investigation on different projections arrangement using parallel beam and fan beam projection techniques.

Numerous researches which utilize optical fiber sensors have shown several successfully cases in flow imaging on low concentration flow of solid particles [2] as well as bubble flow column [5]. In order to increase the flow imag-

ing's resolution in a tomography system, the measurement system must be able to generate a maximum number of possible measurements from the implemented sensor array [6].

The main purpose of this project is to maximize the optical sensors' ability as well as increasing the optical sensors' reliability in process tomography to visualize the solid-gas flow in conveyor. Previous research showed the ability of optical sensors has not fully utilized, where only a single measurement was produced by each pair of sensors [2]. By implementing the switching technique in fan beam projection, an equivalent rotating source in the fourth generation medical X-ray imaging system is obtained [7]. The implementation showed a higher number of measurements, where the number of produced signals equals the number of receivers multiplied by the number of rotating angles (number of emissions). For example, 16 pairs of optical sensors using 16 switching sequences results in 256 measurements covering the sensing area in different directions. The sig-

* Corresponding author. Tel.: +60 7 5535902; fax: +60 7 5566272.

E-mail addresses: ruzairi@fke.utm.my,
ruzairiabdulrahim@yahoo.co.uk (R.A. Rahim).

nals' setting time of receiver together with associated signal conditioning circuit has limit the switching speed of fan beam projections. Therefore, the characteristics of light spectrum's response and stray capacitance effect in optical sensors have to be considered. At the same time, the signals' frequency response and transient response become the main considerations during the construction of signal conditioning system.

2. Hardware design

Usually, a typical tomography system consists of three main units: (1) a sensor, (2) sensing electronics and (3) a computer. The sensor has been designed to interrogate the imaging area from many different viewing angles. The sensing electronics take measurements from the sensor and fed the data to computer. The computer controls the operation of hardware and conducts the image reconstruction at the same time [6].

The same case is applied to the optical tomography system, where the system is being split into three sub-systems; namely the sensor array, signal conditioning circuits and data acquisition system, and computer. Fig. 1 shows the system overview of an optical tomography system. The operation of the system starts with the projection of light into the conveyor while the photo-detector is being used to measure the light irradiance. The output voltage from the photo-detector is generated by an electrical current proportional to the intensity of the received light. Therefore, the generated current depends on the position of the flowing objects within the sensing zone. The electronic circuit is able to measure at least two physical parameters of object flowing in the conveyor. The first measurements is the intensity of received light that is related to the distribution of flowing object, while the second measurement is differential of light related to particle flow rate [8]. The measured data are then transferred to a computer through a data acquisition system (DAS). Computer software is being used to obtain the concentration profile [18], velocity profile [9] and mass flow rate profile of the flow.

In this project, the block diagram of the developed system is shown in Fig. 2. The blocks in blue colour are categorized as analog signal while the blocks in magenta colour are categorized as digital control section. The digital control enables the system to measure the maximum numbers of possible combination measurements in a similar manner to those used in the other process tomography systems such as ECT and EIT. A data acquisition system (DAS) in the form of computer plug-in board using ISA interface has been used to simplify the signal digitization process and personal computer (PC) interface. Two synchronization signals (*Clk* and *Trig*) are used to control the operation of data acquisition and result in accurate sampling hold time and high throughput data acquisition.

3. Selection of optical sensor

In order to select the optimum pair of optical sensor for process tomography applications, it is necessary to consider the characteristics and requirements of the process. Various aspects of consideration are required, including the conveyor's physical characteristics, size of the process (conveyor's diameter), range of conveying rate, type of materials to be conveyed and cost of the designed system [10]. Generally, the implementation of the fan beam projection principle and all possible combinations of an emitter–receiver's output measurements require a very fast switching device to prevent any information being missed and allow the original signal to be reconstructed. Therefore, the selected emitter must have a very fast setting time when drive by a pulsed current while the receiver must have a very fast transient characteristic when exposed to switched light sources.

3.1. Selection of emitter

In previous researches carried by Abdul Rahim, Rzasa and Ibrahim, 2.3 mm diameter polymer fiber optic has been used as the light transmitter. The implementation of fiber optic allowed a large amount of optical fiber sensors being installed around the conveyor which results in increased resolution [3]. In this project, direct implementation of light emitting diodes (LED) as the light transmitter have been used.

Basically, the considerations during selection of LED including the physical size of LED, wavelength (colour) of emitted light, luminous intensity and the direction of emission. The selection of LED has focused on the super bright LED with 3 mm in diameter. This is because a wide range of 3 mm LED are available and the size is considered small compared to common used LED (5 mm in diameter). The implementation of fan beam projection requires the LED with wide radiation angle where the emitted light may cover all the investigated cross-sectional area [11]. The required emission characteristic is illustrated by emitter Tx12 in Fig. 3a, while Fig. 3b shows the small (narrow) radiation angle of LED unable to cover all projection area.

In addition, the emission of the selected LED must have a sufficient luminous intensity (at least 50 mcd) to reduce the signal's setting time of photo-detector and optimizing the detectors output signal. Besides that, the selected LED must be able to support dynamic high current when performed in the switched mode projection. To obtained the high luminous intensity, the selection has focused on indium gallium aluminum phosphide (InGaAlP) type LED due to it provides the highest intensity of emitted light in LED family. Two types of LED have been tested. There are TLOE260A manufacturer by Toshiba Corporation and TLHK4000 manufactured by Vishay Semiconductor. Table 1 shows the comparison of the specifications between TLOE260A and TLHK4000.

An experiment on LED's directional characteristic is carried out to predict the sensor outputs from different angles. The selected photodiodes in Section 3.2 are fixed into the

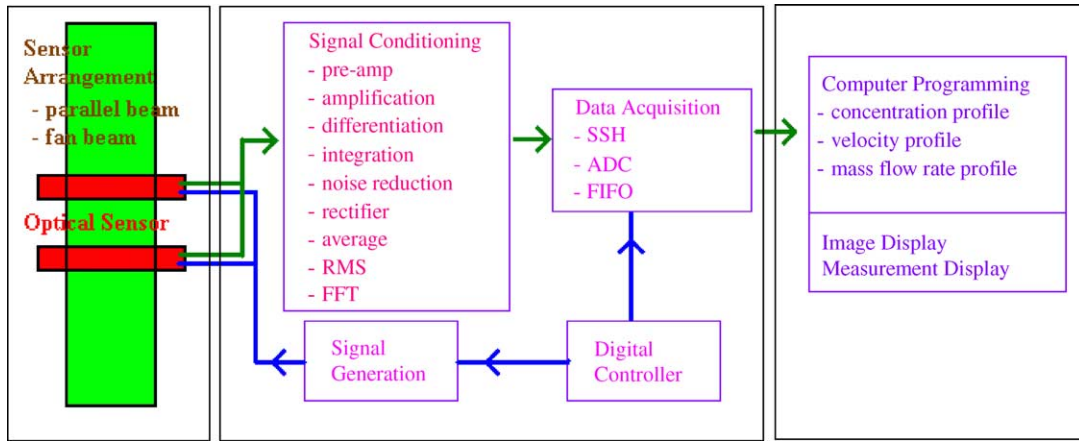


Fig. 1. An overview of an optical tomography system.

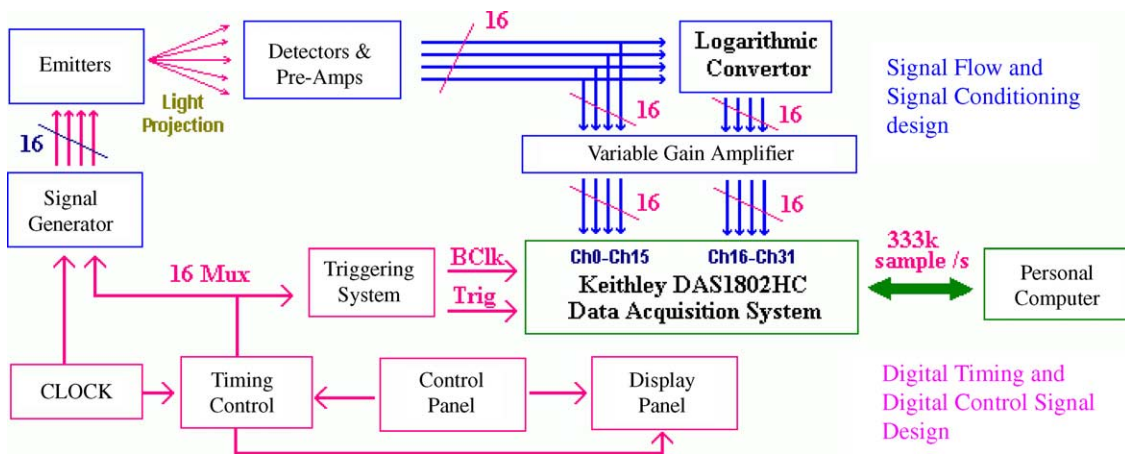


Fig. 2. Block diagram for the developed optical tomography system using fan beam projection technique. (For interpretation of the references to colour in this figure, the reader is referred to the web version of the article.)

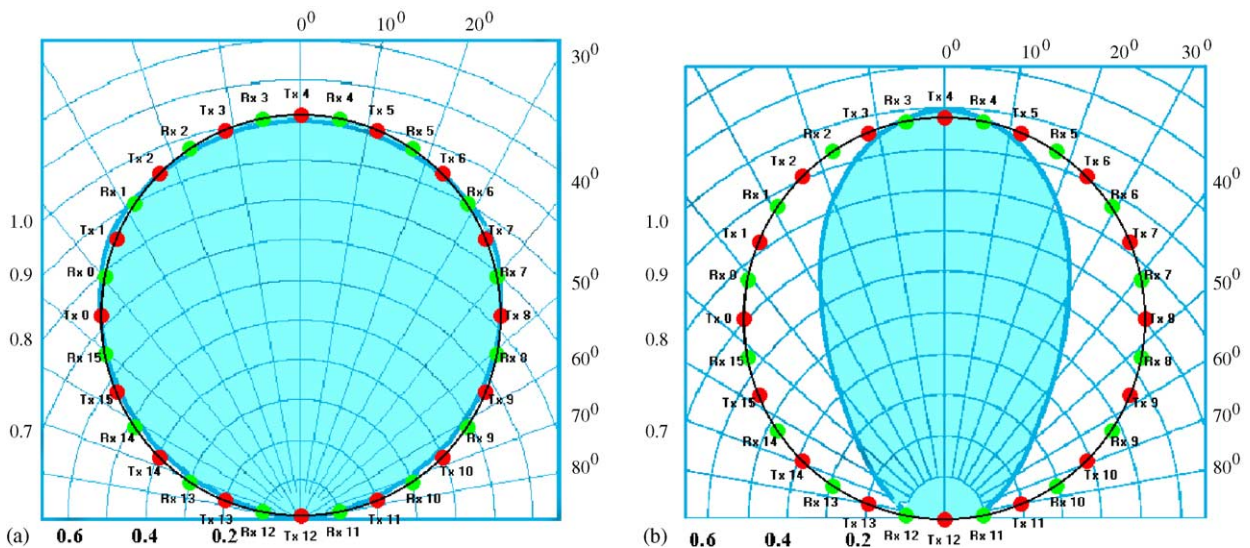


Fig. 3. Light emission angle: (a) wide radiation angle and (b) lesser wide radiation angle.

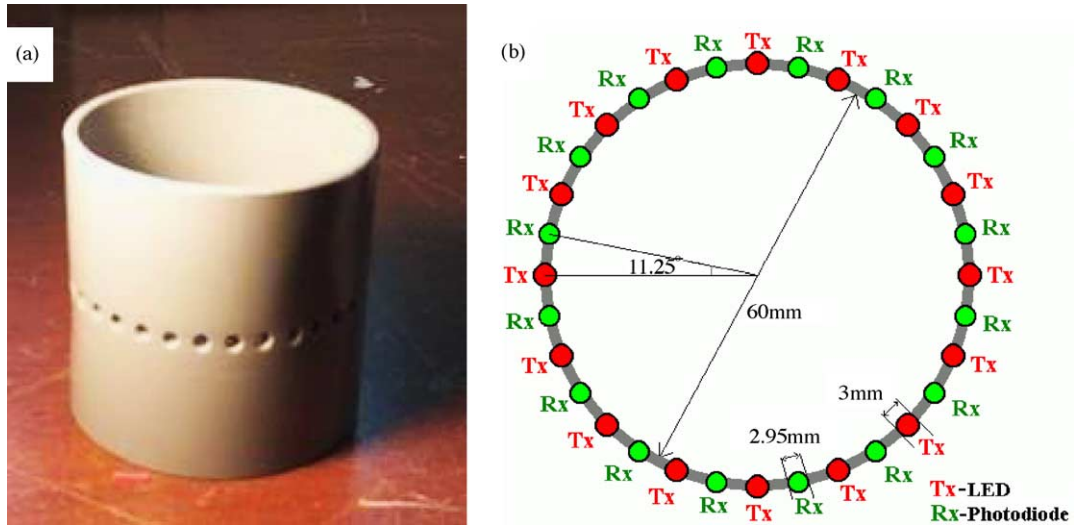


Fig. 4. Sensor fixture: (a) drilled PVC pipe connector and (b) sensors arrangement.

Table 1
Comparison of the specifications between TLOE260A and TLHK4000

Specifications	TLOE260A	TLHK4000
1 Peak emission wavelength, λ_p (nm)	612	647
2 Dominant emission wavelength, λ_d (nm)	605	635
3 Luminous intensity, I_v (mcd), $I_f = 20$ mA	70	120
4 Luminous intensity, I_v (mcd), $I_f = 50$ mA	180	220
5 View angle ($2\theta^{1/2}$)°	140	140

sensor fixture described in Section 4 based on the orientation of receiver shown in Fig. 4b. The receivers are connected to the pre-amp circuit described in Section 5. To test the LED, the selected LED is fixed into the position of Tx0 and a 100 Hz, 50% duty cycle pulse wave driver with 50 mA current supply is supplied to the LED. The peak signal produced in the pre-amp circuit for each receiver is observed through the use of oscilloscope. The results obtained by using TLOE260A and TLHK4000 are tabulated in Table 2.

From Table 2, it is found that the TLHK4000 produced a better result. The emission intensities in the covered directions are more uniform where the produced signals are similar to the modelling reference voltages. Besides that, the

amplitudes are higher compared to TLOE260. Therefore, the TLHK4000 has been selected as the light sources for the sensor system.

3.2. Selection of light detector

In the light detector family, there are a wide range of different light spectrum photo sensors. To obtain an optimized and accurate reading, the selection of light detector must be unique to the exposed light spectrum and provide a fast setting time. In addition, the type of detector selected must consider the detector’s noise limit (smallest signal that can be handled), leakage current, mating electronics, packaging constraints, signal-to-noise ratio, frequency bandwidth and the cost [14].

In this project, the emitter used is InGaAlP type LED which produces light at 660 nm wavelength. Therefore, the selected photo-detector must be able to provide the peak response at the same wavelength. The selection focused on a photodiode, because it provides a smaller physical size, better stability and linear output, and supports the dynamic range. As a result, the SPC305 PN photodiode which is manufactured by Sanyo Corporation has been selected. The SPC305 is

Table 2
The results obtained from the test of LED’s directional characteristic

	Sensor output voltages (V)							
	Rx0	Rx1	Rx2	Rx3	Rx4	Rx5	Rx6	Rx7
TLOE260A	1.2	3.2	10.0	3.2	2.4	2.8	2.8	4.4
TLHK4000	10.0	0.5	2.5	4.4	6.5	5.0	7.7	10.0
	Rx8	Rx9	Rx10	Rx11	Rx12	Rx13	Rx14	Rx15
TLOE260A	4.5	2.5	3.0	2.3	3.6	10.0	1.9	0.8
TLHK4000	8.4	7.7	7.0	6.5	6.6	2.4	0.4	10.0

2.9 mm silicon PN photodiode and provides the peak response at 630 nm wavelength.

4. Prototype fixture of optical sensor

The development of an optical sensor fixture for the implementation of the fan beam technique become the most critical part in this project due to the need for knowledge of mechanical design and material selection. The considerations during the fixture design include the physical size of sensors and precise of sensor placement. In this project, a 60 mm inner diameter PVC pipe connector is used as the sensor fixture. The use of a PVC pipe connector simplified the fixture to pipe-line installation problem and reduces the cost of fixture development. Sixteen holes 3.0 mm in diameter and 16 holes 2.95 mm in diameter are drilled alternatively around the centre of connector in equal angular distance (refer Fig. 4b). The LEDs are inserted into the 3.0 mm drilled holes while the photodiodes are inserted into the 2.95 mm drilled holes. A two part hardness epoxy is used to fix the inserted sensors on the connector to prevent movement. Fig. 4a shows the drilled PVC pipe connector, while Fig. 4b shows the arrangement of LED and photodiode in the drilled holes on connector.

5. Circuit design

Basically, the developed circuits are divided into three parts, which are light projection unit, received signals conditioning unit and digital timing and control unit. The light projection unit contains a series of LED drivers that provide a high and adjustable dynamic current to each LED individually. In the signals conditioning unit, the received lights' intensity is measured. It contains a series of signal transformation circuits that convert the received signals from the photodiodes to a proportional voltage. The operation of transformation is performed by using a parallel processing technique where 16 sets of such circuit are employed. For digital timing and control unit, a master clock is used to control the sequence of light projection and synchronize the operation of the data acquisition system (DAS) to capture the output voltage from the signals conditioning unit. An important aspect during the circuit development is the considerations of the highest data rate that may be achieved and the stability of signals in each part of the circuits.

5.1. Light projection circuit

This circuit contains 16 similar emitter driver circuits used to drive the individual LED. The emitter is operated in pulse mode because it can handle a larger current and generate a greater intensity of radiation. The circuit is shown in Fig. 5.

To obtain high speed switching and high current driver the ZTX689B NPN transistor was chosen. This transistor has the same characteristic as a Darlington transistor and is able to

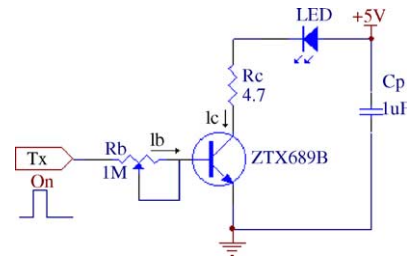


Fig. 5. The emitter driver circuit.

provide the collector with a constant current up to 3 A or a pulse current up to 8 A and support the switching frequency up to 1 MHz. This transistor directly replaces the commonly used LED driver which is formed by a switching transistor and a high current transistor.

Each port in the light projection circuit is connected to a digital timing and control unit which will provide the base of transistor a signal of either high (5 V) or low (0 V). This signal will provide base current I_b , which will turn on the transistor. A $1\text{ M}\Omega$ variable resistor, R_b is used to control the current flow in the transistor's base and indirectly control the current flow in the emitter. A fixed resistor, R_c value $4.7\ \Omega$ is used to protect the emitter from over-current when the I_c exceeds the maximum forward current allowed by emitter. The current flow in emitter, I_c can be determined using equation below

$$I_c = I_b \beta \quad (1)$$

$$I_b = \frac{5}{R_b} \quad (2)$$

where I_c and I_b , the current flow in transistor's collector and base; β , gain of transistor which is equal to 400; R_b , the variable resistor in transistor's base.

The maximum current flow in the emitter, $I_{c\text{ max}}$ occurs when the transistor operates in saturation mode, where the collector current equals

$$\begin{aligned} I_{c\text{ max}} &= \frac{V_{cc} - V_{ce\text{ sat}} - V_F}{R_c} \\ &= \frac{5\text{ V} - 0.5\text{ V} - 2.3\text{ V}}{4.7} = 468\text{ mA} \end{aligned} \quad (3)$$

where $V_{ce\text{ sat}}$, the saturation voltage of transistor which is equal to 0.5 V. V_F , the forward voltage of emitter which is equal to 2.3 V. R_c , the fix resistor at transistor's collector ($4.7\ \Omega$)

The coupling capacitor, C_p is used to smoother the ripple effect from the supply voltage. This circuit is duplicated into 16 sets to get 16 emitter controlling circuit. Since the maximum current flow has exceeded the maximum continuous rating of LED, the design of the driving signal must operate in pulse mode where the average DC current should not exceed 50 mA as given in the data sheet.

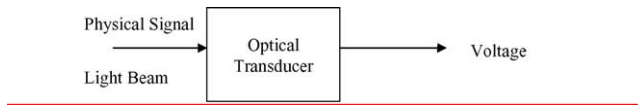


Fig. 6. Optical transducer.

5.2. Signal conditioning unit

The signal conditioning circuit is designed for converting the received signals from the photodiodes to voltages. The input of the sensor is a physical signal represented by light, while the output of the sensor is an electrical signal that is proportional to the intensity of received light as shown in Fig. 6.

The parallel signal processing technique used in the UMIST ECT system [6] has been utilized in this system. This technique assigns each photodiode with a set of optical transducer individually. Hence, the signals conditioning circuit for this project is made up of 16 similar optical transducer circuits. Hence, the signals from photodiodes can be process simultaneously and a fast data rate may be obtained.

Basically, the optical transducer circuit is divided into two parts, which are current to voltage converter (pre-amp) and signal conditioning processing. In the current to voltage converter part, the photodiodes are configured in photovoltaic mode (voltage-output operating mode) [12]. This configuration converts a variable input current (from photodiode) to a proportional output voltage. A basic circuit that accomplishes this is shown in Fig. 7a. In the circuit, the TLE2084 is selected as the converter's operational amplifier (op-amp) due to its high input impedance ($10^{12} \Omega$, J-FET input stage), wide bandwidth (9.4 MHz unity gain bandwidth) and fast slew rate (35 V/us of positive slew rate at 25 °C) compared to TL074 and TL084 op-amp, fast setting time (0.4 us) and low noise voltage (11.6 nV $\sqrt{\text{Hz}}$) at 10 kHz.

Practically, the exposed light on the photodiode's surface causes a small current, I_{Rx} (in the range of μA) to flow through the photodiode from cathode to anode. The high input impedance at the inverting input of the op-amp forces the current flow through the feedback resistor, R_1 . The voltage at

the inverting input of the amplifier follows the voltage at the non-inverting input of the amplifier. Consequently, the output voltage, V_{out} will change in voltage according to the current flow through resistor, R_1 . The transfer function of light to photodiode current in this circuit is equal to:

$$I_{Rx} = \frac{\text{radian flux energy}}{\text{flux}} \quad (4)$$

where I_{Rx} , the current produced by the zero biased photodiode with units in A/cm^2 ; radiant flux energy, the light energy in W/cm^2 , flux, the photodiode's sensitivity with units in W/A , which equals to 5 W/A for SPC305 photodiode.

The pre-amplification converts the current of the photodiode to voltage, which is equal to

$$V_{out} = I_{Rx} R_1 \quad (5)$$

The photovoltaic mode converter has been improved as shown in Fig. 7b. A second resistor with a value equal to the feedback resistor is added in series with the non-inverting input of the op-amp. This configuration results in a differential-input current to voltage converter, which provides a better solution to noise sensitivity and DC offset error [13]. Beside the presence of C_1 as the cumulative parasitic capacitance of R_1 results in the high frequency noise generated by photodiode being filtered. The combination of R_1 and C_1 provided a single low-pass frequency-selective circuit that has a roll of $-20 \text{ dB}/\text{dec}$ above the critical frequency, f_L . The selection of cut-off frequency formed by R_1 and C_1 is based on the maximum frequency to drive the emitters which is expected to be equal to 16 kHz. The determination of C_1 can be calculated using Eq. (6).

$$C_1 = \frac{1}{2\pi R_1 f_L} = \frac{1}{2\pi \times 4.7 \times 10^6 \times 16 \times 10^3} = 2.12 \text{ pF} \quad (6)$$

Due to unavailability value of capacitance 2.12 pF, the 2.0 pF ceramic plate capacitor has been used. This results in the cut-off frequency of low-pass filter to be 16.93 kHz.

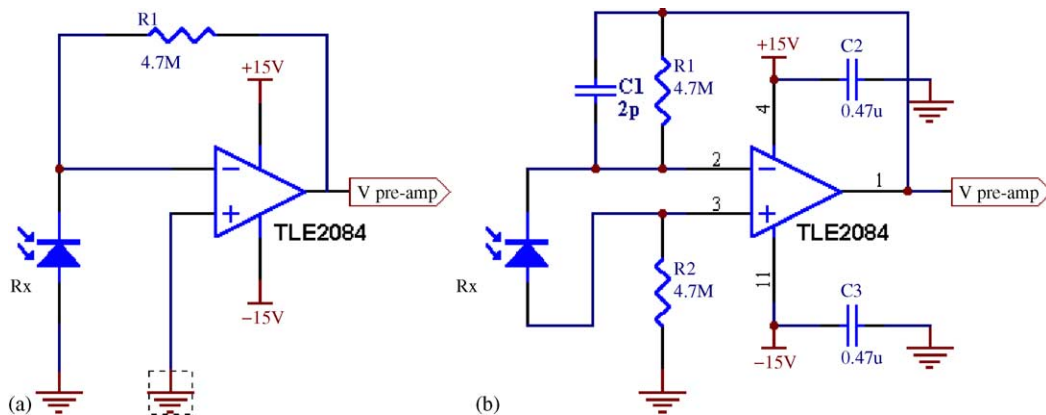


Fig. 7. Current to voltage converter circuit (a) photovoltaic (zero bias) mode and (b) differential-input converter.

To reduce the ripple voltage effect from the power supply, the C_2 and C_3 decoupling capacitors value 0.47 μF are added in parallel with +15 V and –15 V supply [14]. The signal conditioning processing part is formed by a voltage divider, a non-inverting amplifier and a low-pass filter. Fig. 8 shows the schematic of the signal conditioning that performs the signal amplification and filtering.

In the circuit, the output signal from the pre-amp is fed into a 20k preset, VR_1 . The use of preset instead of carbon type variable resistor due to high stability over large range of temperature (± 100 ppm/ $^\circ\text{C}$) and low contact resistance variation (less than 1%). The ability of controlling the level of the amplified signal provides a compatible output signal to interface with the data acquisition system (DAS). For example, when the DAS is programmed for a range of 5 V, the voltage divider can be set to half compared to DAS programmed for a range of 10 V. The output signal from the voltage divider is then fed into a non-inverting amplifier for signal amplification where the gain, A_{ce} is equal to

$$A_{ce} = \frac{R_{20}}{R_{21}} + 1 = \frac{100k}{10k} + 1 = 11 \quad (7)$$

To eliminate the off-set current effect resulting from bias current at the non-inverting input of the op-amp, the resistor R_{19} is added in series between the non-inverting input and the output of preset [15]. The determination of the value of R_{19} is based on the parallel value of R_{20} and R_{21} , which is equal to 9.1 k Ω . To reduce the high frequency noise caused by ambient temperature effect, the same low-pass filter in the pre-amp is added to the feedback resistor of the voltage amplifying stage. The determination of C_9 is based on Eq. (4.7), where C_9 is equal to 100 pF.

5.3. Digital timing and control unit

Generally, the digital timing and control unit is designed to perform two functions. The first function is to control the projection, where the controlled parameters include the frequency of projection, sequence of projection and duration of light emission. The second function is to synchronize the operation of data acquisition by controlling the timing to perform data sampling. An accurate sampling timing is required to obtain the measurement of an output signal in steady-state and increase the projection frequency to maximum.

From experiment, the used optical sensor and signal conditioning unit required an approximately 70 μs of settling time to drive the output signal to achieve steady-state. Fig. 9 shows the dynamic signal captured from receivers Rx12 (yellow in colour) and Rx13 (blue in colour) for projection Tx0–Tx4 in experiment. The positive edge of green colour signal represented the start of each projection while the negative edge occurs when the signal achieved the steady-state for corresponding projection.

In this project, the DAS used provided a maximum data sampling rate at 333k samples per second, which means conversion of a single sample required 3 μs . Since 16 sensors

are used, a single projection will provide 16 output signals. Therefore, 48 μs of data sampling time is required to complete the conversion of these analogue signals. Hence, the minimum interval between the projections is approximately equal to 118 μs (70 μs + 48 μs) and the allowed maximum projection frequency is equal to 8474 Hz (1/118 μs). Since 16 emitters are used, 16 projections are required in order to complete a full measurement cycle and 256 signals are obtained from the signal conditioning circuit. As a result, the developed system is able to provide a maximum of 529 data set per second (8474/16) for the computer. Due to slow image processing rate, the projection frequency has reduced to 4.8 kHz in order to optimize the direct memory transfer in computer. In the software programming, the DAQ has been programmed to operate in DMA mode, the DAQ will automatic update the allocated memory every 33 ms which consists of the latest 10 frame of measurement. Fig. 10 shows the designed timing diagram for projection and operation of data acquisition.

Each signal in Fig. 10 plays an important role in specific functions to achieve synchronization. The *Clk* signal is the base signal to drive the *Trig*, *BClk*, *LED_On* signals and control the sequence of light projection. The first rising edge of *Clk* signal will switch on the emitter Tx0, continued by Tx1 and ended by Tx15 for a complete cycle. The falling edge of *Trig* signal is used to trigger the DAS to stand by for a new cycle of projections' signals conversion operation. The falling edge of the *BClk* signal triggers the DAS to perform the data conversion from channel-0 to channel-15 where the sensors output signals are connected. The DAS has been programmed to be ready for conversion after receiving the falling edge of *Trig* and to stop the conversion when complete the conversion for the 16th falling edges of received *BClk*. The *LED_On* signal is used to control the duration of emitter being light on.

To generate the *Clk* signal with a frequency of 4.8 kHz, a 555 timer configured in astable mode is sufficient. The *Clk* signal's generator schematic is shown in Fig. 11 where the output signal's frequency is given by the following equation.

$$f_{Clk} = \frac{1.44}{(R_A + 2(R_B + VR_T))C_T} \quad (8)$$

Based on Eq. (8) and selected values of R_A and C_T in the schematic, the value of $R_B + VR_T$ must be 65.68 k Ω to obtain the chosen output signal's frequency. The value of 65.68 k Ω is obtained with a fixed resistor, R_B and a variable resistor, VR_T . In the circuit, the VR_T variable resistor is a 25-turn cermet trimmer to adjust and fix the frequency of *Clk* at 4.8 kHz. The use of multi-turn cermet trimmer provides an accurate trimming resistor and stability over a large range of temperature.

To obtain the sequential projections of 16 emitters, a four-bit binary counter and a 4- to 16-line decoder are used. The binary counter is configured to operate in free running mode where each rising edge of the *Clk* signal results in one bit increment of counter output. The binary bits output from the

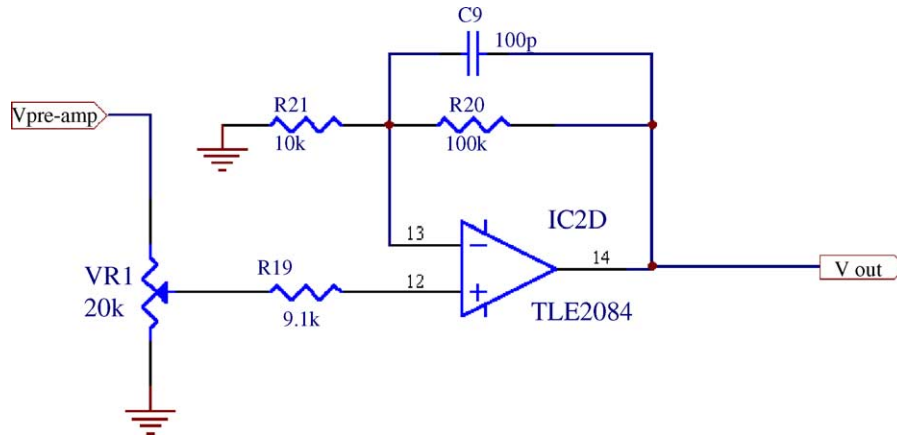


Fig. 8. Schematic of linear voltage converter.

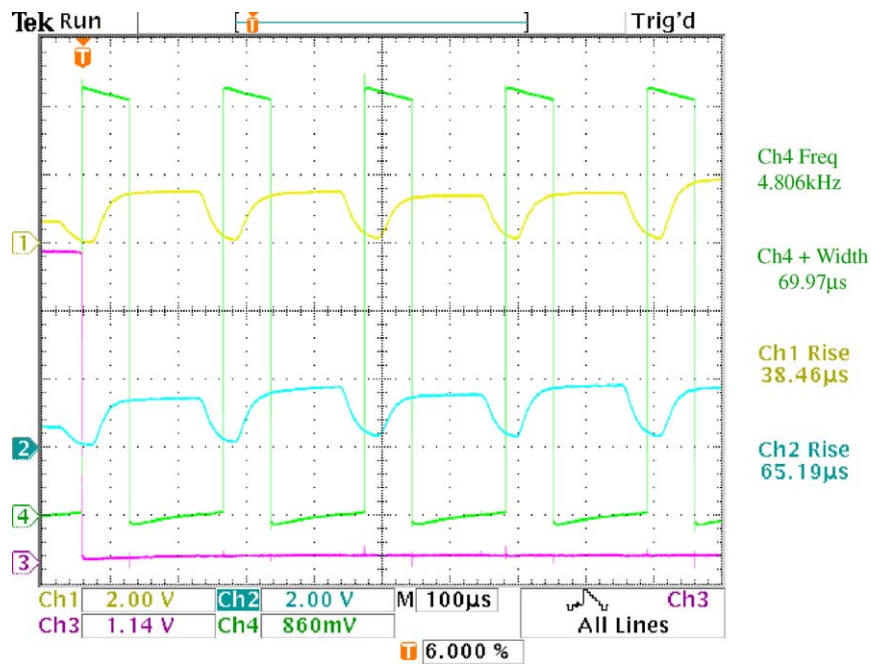


Fig. 9. Approximately 70 μ s is required by signals to achieve steady-state. (For interpretation of the references to colour in this figure, the reader is referred to the web version of the article.)

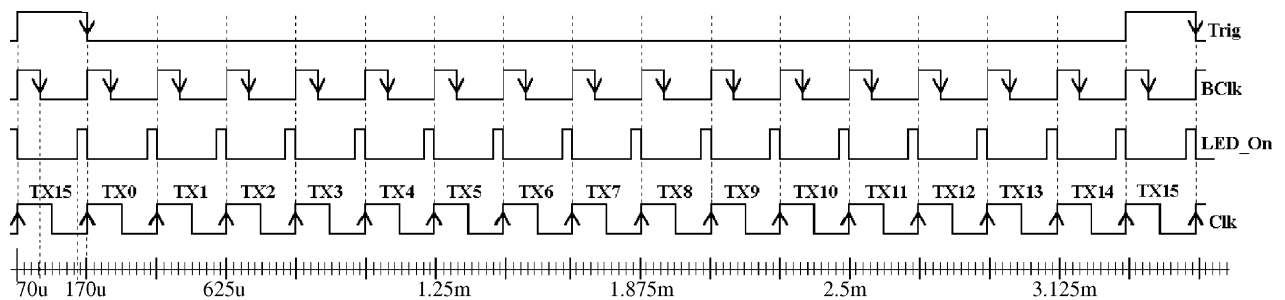


Fig. 10. Digital timing and control signals.

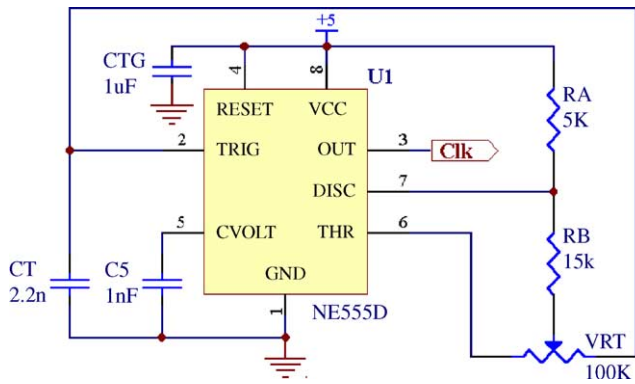


Fig. 11. Clk signal's generator schematic.

counter are decoded using a 4- to 16-line bit decoder. Since the decoded outputs are active low, an inverter is added to each output line of the decoder. The schematic diagram is shown in Fig. 12. The duty cycle of each output line of the decoder is fixed at 6.25% ($1/2^4 \times 100\%$) with a frequency 300 Hz ($4.8\text{kHz}/2^4$), which means the duration of optical emission is equal to 208 μs ($1/300\text{Hz} \times 6.25\%/100$). From the pre-determined minimum duration of a projection, only 118 μs are required to complete the measurements of a projection. Hence, to obtain a better performance from the LED, minimizing the emission duty cycle is necessary to reduce the heat produced by the LED. This will result in a stable luminous intensity over permitting a time, higher forward current being used, fully turn off the LED before the next projection occurs and automatically initialize the signal conditioning circuit before processing the signals produced by the next projection. To solve this problem, a monostable multivibrator is used to generate the LED_On signal. This signal allows the duty cycle of each projection to be manipulated by controlling the duration of the enable pin ($\overline{G1}$) of decoder being 'low'. In this project, the duration of the emission is 120 μs with the duty cycle equal to 3.6%. To obtain this dura-

tion, a precise RC configuration of monostable multivibrator is required. The equation of duration of the output signal, T_w from the monostable is given as below.

$$T_w = KR_x C_x \tag{9}$$

where R_x in $k\Omega$ ($R_{E1} + VR_{E1}$ in Fig. 12), C_x in pF (C_{E1} in Fig. 12), T_w in ns while k is a constant equal to 0.37. Theoretically, to obtain a monostable output with 133 μs pulse width where the C_x is 4.7 nF, the required R_x is equal to

$$R_x = \frac{133 \times 10^3}{0.37 \times 4.7 \times 10^3} k\Omega = 76.48 k\Omega$$

R_x is formed by a fixed resistor (R_{E1}) and multitrurn cement trimmer (VR_{E1}). Practically, the trimmer is set to the required frequency by observing the pulse width measurement using an oscilloscope. The enable pin to decoder is active low so the inverting pin of a monostable multivibrator is used. The full schematic of the light projection control unit is shown in Fig. 12.

As mentioned above, the BClk and Trig are used to synchronize the data acquisition. The falling edge of BClk can only occur when the processed signals in the signal conditioning circuit achieve steady-state, which is approximately equal to 70 μs . While for Trig signal, the falling edge must occur when the first projection is obtained and before the first falling edge of BClk, otherwise the conversion of the first projection data will be skipped by DAS. To generate the Trig and the BClk signals, the same device as LED_On's signal is used, hence, a triggering source is required for each signal. The frequency of the triggering source must have the same frequency as the generated signal. For BClk signal, the base signal, Clk was selected as triggering source while for Trig signal, the counter overflow signal (SOC) is selected. The SOC signal was generated by a counter when the accumulator of the counter overflowed (1111_2 or $0x0F$). In this project, the BClk signal has been set to 70 μs while the Trig is set to 205 μs . The schematic of the BClk and Trig generator is

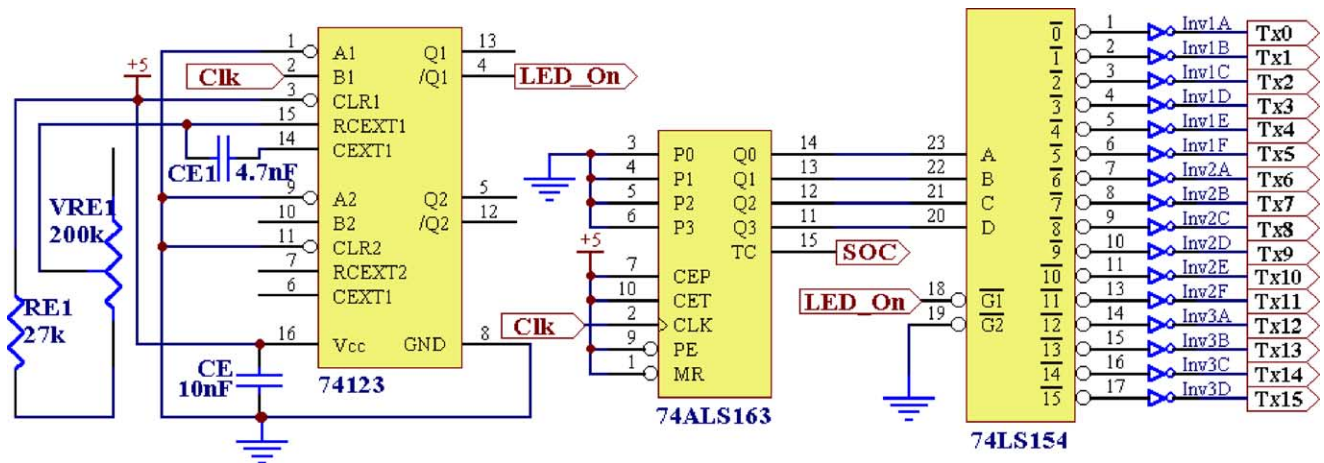


Fig. 12. The schematic of light projection controlling unit.

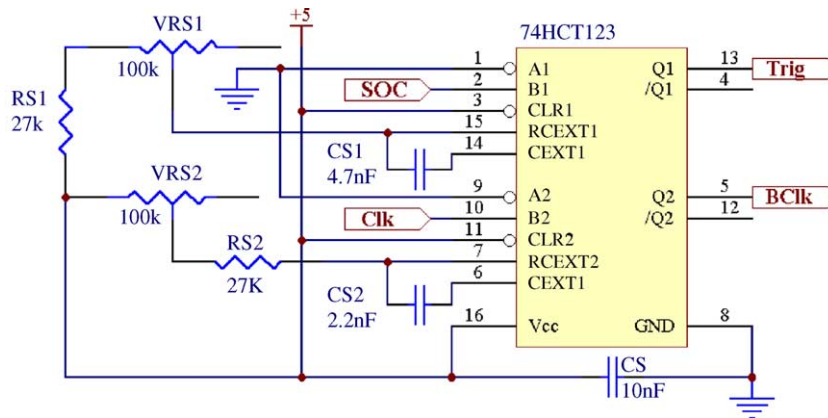


Fig. 13. Signal generator for Trig and BClk.

shown in Fig. 13. The VR_{S1} and VR_{S2} are adjusted to obtain the decided pulse length. Fig. 14 shows the generated signal for Trig, BClk and Clk and LED_On signals that are captured with an oscilloscope.

6. Data acquisition system

Real-time image reconstruction needs an interface to send the output signal from the hardware system (analog) to the computer (digital). Practically, the gateway can be done by using either a computer serial communication port such as USB, RS232 and Ethernet or a parallel port such as a printer port. However, the input signal must be digitized in the hardware system before going through these ports. To digitized the signal may need a complex circuit to be built on the hardware system and result in time consuming and complex trouble shooting procedures. To speed up the development, the interfacing can be performed by using an industrial standard computer data acquisition system (DAS). The use of

DAS simplified the procedure of data acquisition the analog signals are wired directly to the DAS terminal. The general functions provided by the industrial standard DAS includes multiple channels switching capacity, analog to digital converter (ADC), digital to analog converter (DAC), digital input (DI), digital output (DO), operation of computer interrupt and direct memory access (DMA) and storage of acquired data. In this project, the Keithley Metrabyte DAS1802HC has been used.

7. Image reconstruction algorithm

To reconstruct the cross-sectional image from the projection data, the back projection algorithm has been used. The measurements obtained at each projection are projected back along the same line, assigning the measured value to each point in the line. This assumes equal probability of the object contributing to a point along the ray that produced that point. The values are smeared back across the unknown den-

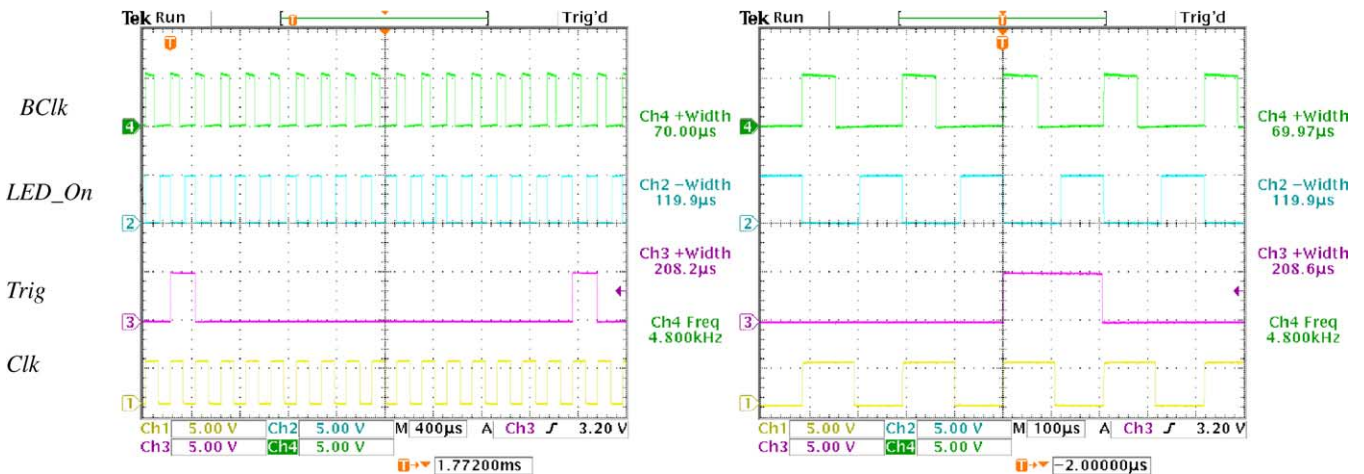


Fig. 14. The generated signal for Clk, Trig, BClk and LED_On.

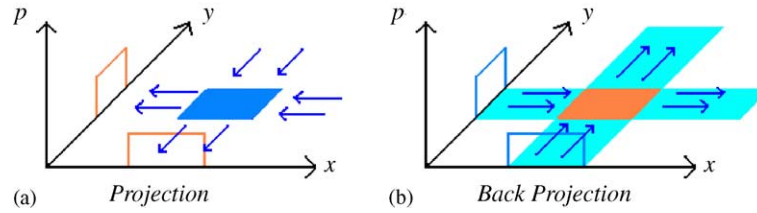


Fig. 15. (a) Projections to a rectangular object are measured in the x and the y directions. (b) These measurements are then projected back to form an image.

sity function (image) like a line of wet paint from a brush. The process of back projection is shown in Fig. 15 for an image consisting of a single central area and the projection x and projection y are identical.

In this project, the linear back projection (LBP) algorithm has been used to perform the image reconstruction. The concentration profile is generated by combining the projection data from each sensor with its computed sensitivity map [5]. The modelled sensitivity matrices are used to represent the image plane for each view. To reconstruct the image, each sensitivity matrix is multiplied by its corresponding sensor reading. This is same as back projecting each sensor reading on to the image plane individually. As the result, $m(n \times n)$ matrices are obtained, where m is the number of obtained projection data, while n is the reconstructed image resolution or dimension of the sensitivity matrix used. The same elements in these matrices are summed to provide the back projected voltage distributions. This process can be expressed mathematically as below

$$V_{\text{LBP}}(x, y) = \sum_{\text{Tx}=0}^{15} \sum_{\text{Rx}=0}^{15} S_{\text{Rx},\text{Tx}} \overline{M}_{\text{Tx},\text{Rx}}(x, y) \quad (10)$$

where $V_{\text{LBP}}(x, y)$, voltage distribution obtained using LBP algorithm (concentration profile in unit volt) an $n \times m$ matrix where n equals to dimension of sensitivity matrix; $S_{\text{Rx},\text{Tx}}$, signal loss amplitude of receiver Rx-th for projection Tx-th in unit of volt; $\overline{M}_{\text{Tx},\text{Rx}}(x, y)$, the normalized sensitivity matrices for the view of Tx–Rx.

8. Results and discussions

In order to investigate the accuracy of the modelling, four flow models are considered:

- i. A single pixel within the pipe is assumed to be affected by the flowing medium. Three different sizes of flow objects are investigated. This model is used to test the precision of reconstruction algorithm.
- ii. Four pixels within the pipe are assumed to be affected by the flowing medium. This model can be used to test the aliasing effect.
- iii. Half flow where all the pixels on one side of the pipe diameter are assumed to be equally affected by

the flowing medium whereas the remaining pixels are unaffected.

- iv. Full flow where all the pixels within the pipe are equally affected.

In the single pixel flow model (SPFM), the contribution of the flowing object's size in the reconstructed image is investigated. The selected flowing objects' size is based on a single pixel's size in the image plane of resolution 8×8 ($\approx 2\%$ of total sensing area), resolution 32×32 ($\approx 0.125\%$ of total sensing area), and resolution 128×128 ($\approx 0.0078\%$ of total sensing area). In the multiple pixels flow model, four pixels in the image plane are assumed to contain objects. The size of the object is assumed equal to the pixel's size in the image plane of resolution 16×16 (16.06 mm^2 or $\approx 0.5\%$ of the total sensing area, representing the size of a plastic bead). For the half flow model, the left-hand side of the pipe is filled with particles. While for full flow model, the whole pipe contains particles. No light is transmitted through the flowing medium. Hence, for this model, the amplitude of the signals loss is equals to the sensors reference voltage. Fig. 16 shows the size and position of all flow models in the investigated area.

Fig. 17 shows the reconstructed images with resolution 32×32 obtained using the linear back projection algorithm. These images are reconstructed using the modelled projection data for these flow models [16].

In the first three images, the results show an object being reconstructed at the targeted position and the size of object is clearly differentiated in among the flow models. The back-projected shadow of the object has been minimized and smeared through the large number of projection data. The density in the whole image also clearly defines the object distribution profile in the investigated cross-sectional area.

For the multiple pixel flow model, the algorithm has proved satisfactory where all the modeled objects are reconstructed at their targeted positions and the density of each object are uniform and similar to each other. By comparing to the single pixel flow model, the size of flowing objects are reconstructed accurately.

In half flow and full flow models, the images show the weakness of the linear back projection algorithm where the concentration profiles are non-uniform [17]. To solve the problem, the filtered back projection algorithm has been introduced [17].

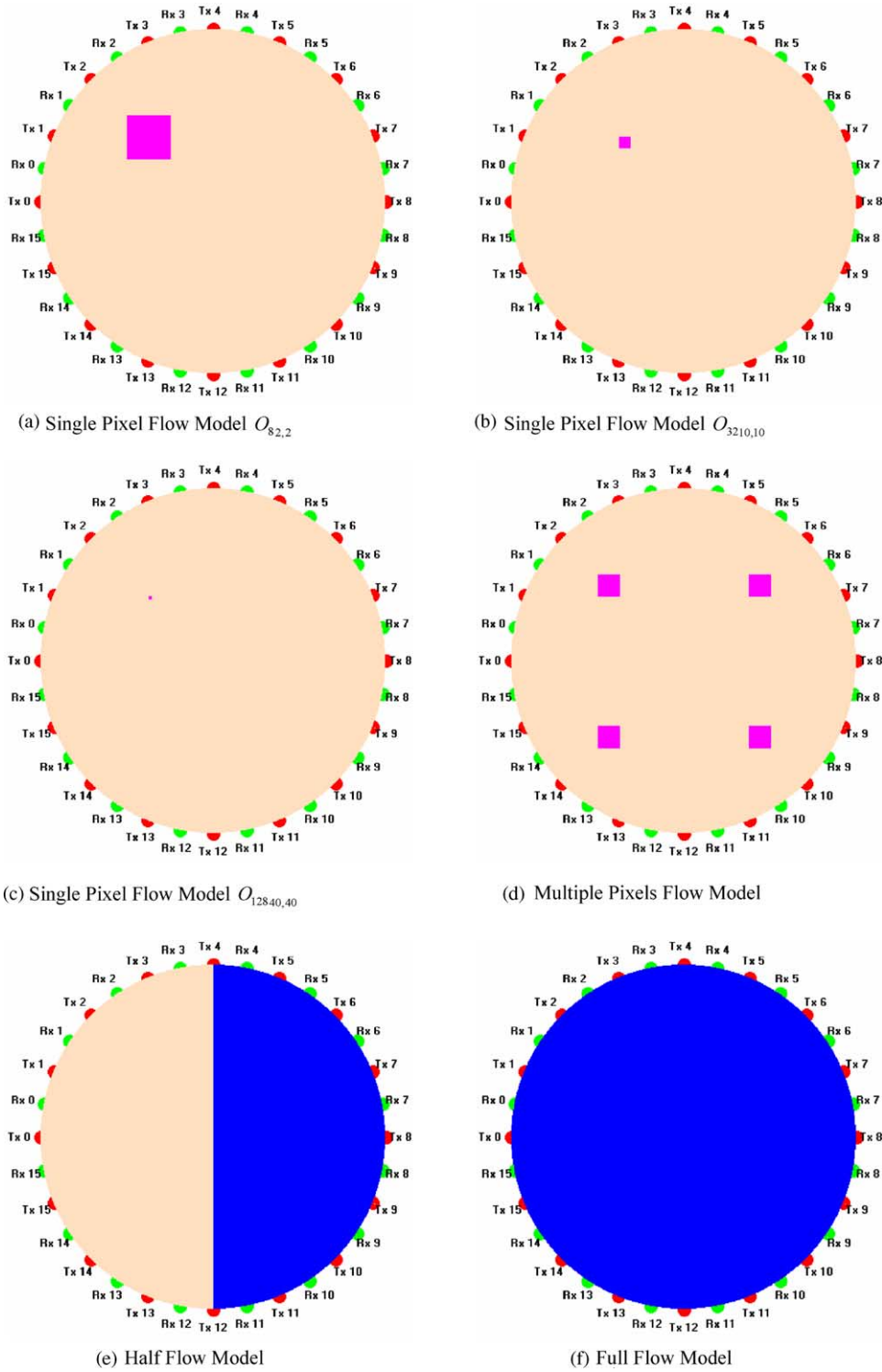


Fig. 16. Size and position of six types flow models.

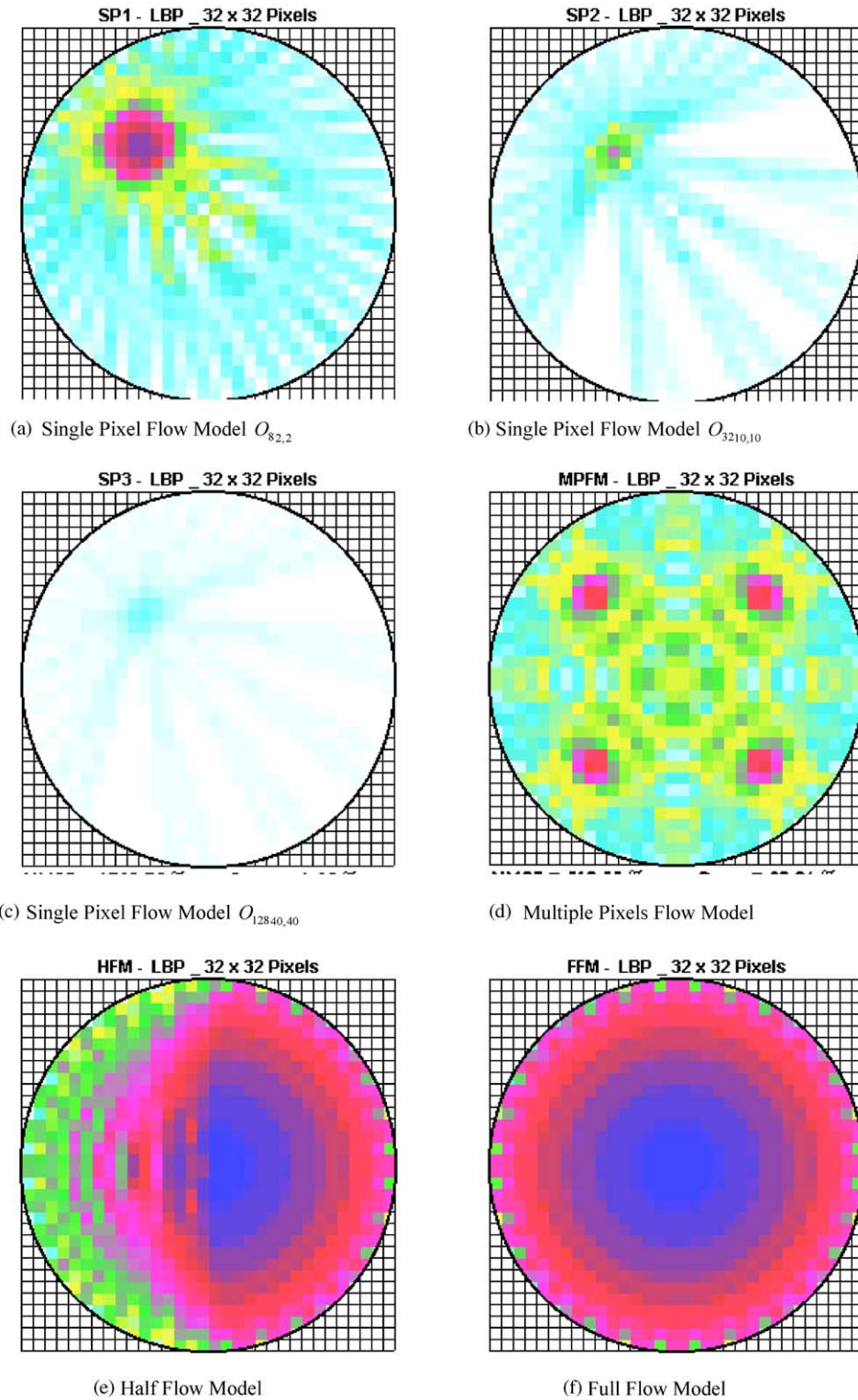


Fig. 17. Reconstructed images for modelled flow models.

9. Conclusion

A developed fan beam based optical tomography system has been discussed. The obtained concentration profile shows the accurate information regarding the object space in the investigated area. By using the linear back projection algorithm with the modeled sensitivity matrices, the modeled sensors output for various flow condition are proved accurately through the inspection on reconstructed image.

References

- [1] W.P. Dugdale, An optical instrumentation system for the imaging of two-component flow, University of Manchester, Ph.D. Thesis, 1994.
- [2] R. Abdul Rahim, A tomography imaging system for pneumatic conveyors using optical fibres, Sheffield Hallam University, Ph.D. Thesis, 1996.
- [3] S. Ibrahim, R.G. Green, Optical tomography for imaging process flow, in: Proceedings of the MSTC 2001, Melaka, Malaysia, 8–10 October, 2001, pp. 149–155.
- [4] R. Rzasz Mariusz, B. Dobrowolski, Evaluation of accuracy of reconstruction of air bubble shape in the computer-assisted of liquid aeration, in: Proceedings of the 1st International Symposium On Process Tomography, Jurata, 2000.
- [5] S. Ibrahim, Measurement of gas bubbles in a vertical column using optical tomography, Sheffield Hallam University, Ph.D. Thesis, 2000.
- [6] W.Q. Yang, DSP/micro-controllers in tomography system—a brief review, in: Proceedings of the International Conference on Embedded systems, Tsinghua University, Beijing, China, 2001.
- [7] W.R. Hendee, E.R. Ritenour, Medical Imaging Physics, third ed., Mosby Year Book, 1995, pp. 414–428.
- [8] K.S. Chan, Offline Image Reconstruction for Optical Tomography, Universiti Teknologi Malaysia, B.E. Thesis, 2001.
- [9] M.A. Khalid, Real-time velocity measurement for optical tomography, Universiti Teknologi Malaysia, B.E. Thesis, 2002.
- [10] K.S. Chan, R.A. Rahim, Optical tomography sensor configuration, in: Proceedings of the World Engineering Congress 2002, Sawarak, Malaysia, 22–25 July, 2002, pp. 323–327.
- [11] A.C. Kak, M. Slaney, Principle of Computerized Tomographic Imaging, IEEE Press, The Institute of Electrical and Electronics Engineers Inc., New York, 1999.
- [12] W. Kester, S. Wurcer, C. Kitchin, High Impedance Sensors Practical Design Technique for Sensor Signal Conditioning, Analog Device Inc., 1998, pp. 5.1–5.40.
- [13] G.G. Jerald, Photodiode Amplifier—Op Amp Solutions, McGraw-Hill, New York, 1996.
- [14] W. Jung, W. Kester, B. Chestnut, Power Supply Noise Reduction and Filtering—Hardware Design Techniques Practical Design Technique For Sensor Signal Conditioning, Analog Device Inc., 1999, pp. 10.21–10.38.
- [15] J.C. Josept, Linear IC Applications—A Designer's Handbook, Butterworth-Heinemann Ltd., Oxford, 1996.
- [16] A.R. Rahim, K.S. Chan, J.F. Pang, L.C. Leong, Optical tomography system using switched mode fan beam projection: modelling techniques. *J. Opt. Eng.*, submitted for publication.
- [17] R.G. Green, M.F. Rahmat, K. Evans, A. Goude, M. Henry, J.A.R. Stone, Concentration profiles of dry powders in a gravity conveyor using an electrodynamic tomography system, *Meas. Sci. Technol.* 8 (1997) 192–197.
- [18] K.S. Chan, A.R. Rahim, Tomographic imaging of pneumatic conveyor using optical sensor, in: Proceedings of the World Engineering Congress 2002, Sawarak, Malaysia, 22–25 July, 2002, pp. 305–309.

Biography



Associate Professor Dr. Ruzairi Hj. Abdul Rahim received his first degree in BEng. Electronic System and Control Engineering in 1992 from Sheffield City Polytechnic, UK. He received his PhD in Instrumentation Engineering from Sheffield Hallam University, UK in 1996. Currently, he is a Head of Department, Control and Instrumentation Engineering in Faculty of Electrical Engineering, Universiti Teknologi Malaysia. His current research interests are process tomography and process measurement.